Characterization and Corrections of Relative Humidity Measurement from Meteomodem M10 Radiosondes at Midlatitude Stations

JEAN-CHARLES DUPONT

Institut Pierre Simon Laplace, École Polytechnique, UVSQ, Université Paris-Saclay, Palaiseau, France

MARTIAL HAEFFELIN

Institut Pierre Simon Laplace, École Polytechnique, CNRS, Université Paris-Saclay, Palaiseau, France

JORDI BADOSA

Laboratoire de Météorologie Dynamique, École Polytechnique, CNRS, Sorbonne Université, ENS PSL Research University, Palaiseau, France

GAELLE CLAIN, CHRISTOPHE RAUX, AND DAMIEN VIGNELLES

Meteomodem, Ury, France

(Manuscript received 27 November 2018, in final form 9 March 2020)

ABSTRACT

Measurement of water vapor or humidity in the atmosphere is fundamental for many applications. Relative humidity measurements with a capacitive sensor in radiosondes are affected by several factors that need to be assessed and corrected. This work aims to address corrections for the main effects for the Meteomodem M10 radiosonde as a step to meet the Global Climate Observing System (GCOS) Reference Upper-Air Network (GRUAN) requirements. The considered corrections are 1) the calibration correction; 2) a slow regime due to the slow diffusion of molecules through the sensor, especially at very high and very low relative humidity conditions; 3) the relative humidity sensor dependence on the gradient of temperature; and 4) the time lag at cold temperatures, which affects measurements in regions of strong relative humidity gradients. These corrections were tested for 26 nighttime and 25 daytime radiosondes in two midlatitude locations for which both Meteomodem M10 and Vaisala RS92 measurements were available. The results show that, after correcting for the four effects, M10 relative humidity measurements are, on average, consistent with the Vaisala RS92 relative humidity values within 2% RH at all altitudes for the nighttime launches (against 6% RH before the correction) and within 5% RH at all altitudes for the daytime launches (against 9% RH before the correction).

1. Introduction

Measurement of water vapor or humidity in the atmosphere is fundamental for many applications (Bojinski et al. 2014). Humidity measurement at higher altitude is still among the most difficult problems in basic meteorology (Elliott et al. 2002): the measurement depends on the exchange of water molecules between the sensor and the air, and during the sounding water vapor concentrations decrease by several orders of magnitude between the surface and the tropopause. Accurate humidity measurements from the ground to the top of the troposphere and lower stratosphere are necessary to prevent spurious drying or moistening of the atmosphere simulated in numerical weather prediction models (Seidel et al. 2009). Such measurements are also necessary to better understand the role of water vapor in climate feedback, to study the life cycle of anthropogenic clouds such as contrails, and to quantify the state of deliquescence of atmospheric aerosols, just to name a few among many other fields of investigation. Moreover, vertical profiles of temperature and humidity can be used to calibrate (error and uncertainty) different types of satellites with active and passive remote sensing instruments (Zou et al. 2013).

Corresponding author: Jean-Charles Dupont, jean-charles.dupont@ipsl.polytechnique.fr

DOI: 10.1175/JTECH-D-18-0205.1

Today, the most widely used atmospheric humidity measurements rely on capacitive sensors that are based on a dielectric polymer deposited between two electrodes. The change in the dielectric constant of the polymer is directly proportional to the change in relative humidity, especially in the 5%–95% relative humidity range (Balagurov et al. 1998). Some instruments also use sensors that are based on the impedance of conductive polymers, which shows an exponential relationship to relative humidity. Capacitive sensors are typically preferred because of a lower sensitivity to temperature of the absolute calibration (Matsuguchi et al. 1998).

The relative humidity measurement accuracy is generally considered to be 2%–5% RH, and this variability is due to 1) errors in absolute calibration; 2) efficiency of the diffusion of water vapor molecules inside the sensor; 3) capacitance sensor response time, which ranges from seconds to minutes depending on temperature; and 4) bias due to spurious heating or cooling of the capacitance sensor relative to ambient air.

All these effects on relative humidity measurements must be well understood and accounted for to characterize measurement accuracy. Each error and its correction has an associated uncertainty that have been carried out and published for several Vaisala, Inc., radiosonde sensors (RS80: Miloshevich et al. 2001, 2004; RS92: Vömel et al. 2007; Dirksen et al. 2014), and for the Meisei Electric Co., Ltd., radiosondes (RS-11G and IMS-100: Kizu et al. 2018).

In the framework of the Global Climate Observing System (GCOS) Reference Upper-Air Network (GRUAN), Dirksen et al. (2014) propose methods to correct Vaisala RS92 relative humidity measurements and to provide measurement uncertainty estimates. Such methods are applied to improve data quality at all GRUAN stations that use RS92 radiosondes. Similar investigations should be carried out on other relative humidity sensors of radiosondes used in the GRUAN network. At least two stations of the GRUAN network (Paris, France and Réunion in the southern Indian Ocean) use Meteomodem Co. M10 radiosondes for regular temperature and relative humidity profiling.

The aim of this paper is to identify error sources that can lead to dry or wet bias and uncertainties. This paper presents a set of corrections that aim at reducing this bias and uncertainties using intercomparison measurement with the RS92. Section 2 presents the dataset used in the study and provides a description of each of the correction methods. Section 3 discusses the impact of each correction on M10 measurements and describes the general result when compared with RS92 measurements. Section 4 presents the sensitivity of measurement bias and standard deviations to different values of correction parameters.

FIG. 1. The Meteomodem M10 radiosonde and its receiver SR10.

2. Observational dataset

To test correction methods and evaluate their effects on measurement accuracies, we looked for a dataset that contains a significant number of both nighttime and daytime dual-radiosonde profiles that include M10 radiosondes and another well characterized radiosonde that can serve as reference, both under the same balloon. This well characterized radiosonde is here defined as a radiosonde for which there exist published studies on its accuracy and on its measurement uncertainties. This is the case for Vaisala RS92 radiosondes, which have been extensively tested (Dirksen et al. 2014). For this study, the data from two field experiments, which are presented in the following subsections, are considered.

a. Meteomodem M10 radiosonde

The M10 is one of the radiosonde commercialized by Meteomodem. The M10 was released in 2010, and it is fully compatible with the SR10 receiver system and the Meteomodem software (Fig. 1). Its dimensions are 95 mm × 95 mm × 88 mm for 150 g with batteries. The M10 is composed of a capacitive humidity sensor covered by an innovative metal coated shield that allows good ventilation while protecting it from direct radiation and from water droplet freezing on the sensor, a temperature sensor that measures the air temperature and positioned at the very end of the sensor boom, and a GPS sensor whose coordinates are measured and from which the pressure, the vertical velocity, the wind speed and direction are derived. The capacitive humidity sensor is composed of three primary components: a basic layer that acts as an electrode; a dielectric material, whose characteristics are a function of relative humidity; and a fast response porous electrode that acts as the

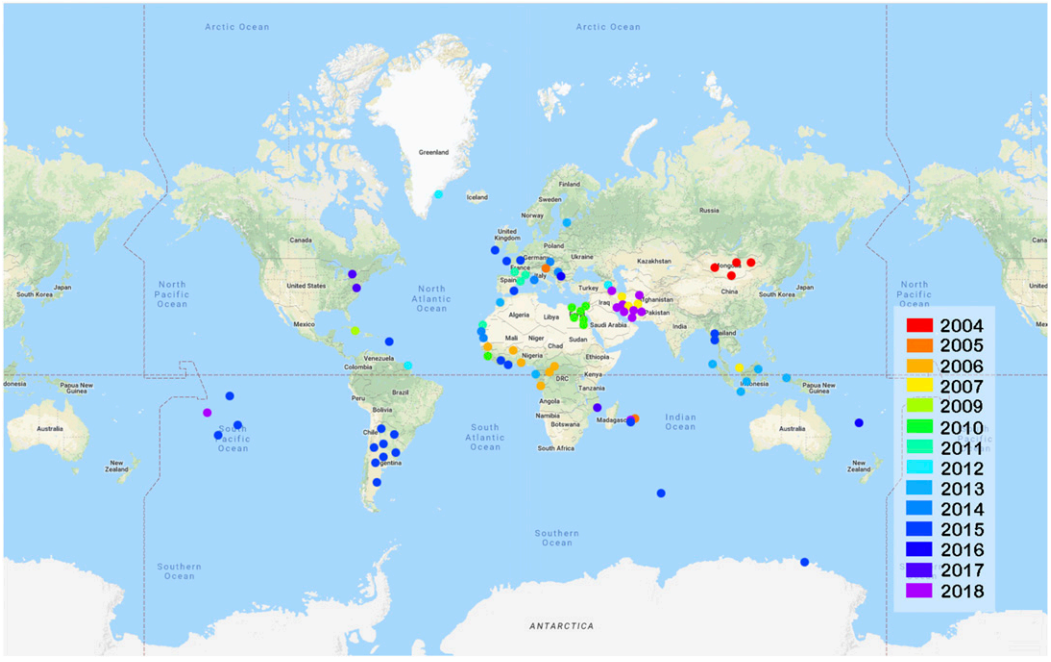

FIG. 2. Locations of all active sites using Meteomodem radiosonde technology in 28 countries; colors indicate the year of the station deployment. All Meteomodem stations installed since 2011 use the M10 technology. Before 2011, sites used the former version of M10 (M2K2) and by now are using the M10 technology. Most of these sites produce two M10 radiosoundings per day.

second electrode of the capacitor. A second thermistor is located under the protective shield close to the humidity sensor in order to have an approximative measurement of the temperature of the capacitive humidity sensor. The UPSI France Company is the subcontractor for this capacitive humidity sensor and these sensors are made specifically and exclusively for Meteomodem. Figure 2 shows the localization of all active sites using Meteomodem radiosonde technology in 28 countries, colors are relative to the year of the station deployment. All Meteomodem station installed since 2011 use the M10 technology. Before 2011, sites used the former version of M10 (M2K2), and by now all are using the M10 technology. Most of these sites produce two M10 radiosoundings per day.

b. *OHP field experiment*

The Observatoire de Haute Provence (OHP) field experiment was dedicated to the improvement of humidity sounding techniques [named Development of Methodologies for Water Vapor Measurement (DEMEVAP); Bock et al. 2013]. It took place at the Observatoire de Haute Provence, in France, during September–October 2011. Four types of radiosondes (Vaisala RS92, Meteomodem M2K2-DC and M10, and Meteolabor AG Snow White) were tested during 20 nighttime radiosonde launches. Raman lidar water vapor measurements, ground-based sensor measurements and GPS-based water vapor observations were also performed during 16 clear sky nights. Bock et al. (2013) found a dry bias for M10 observations of −6.5% RH in the altitude range of 1–12 km and increasing to −10% RH at 10 km when compared with Meteolabor Snow White.

For that study, only calibration-related corrections were applied to the M10 measurements, as the M10 radiosondes had been released shortly prior to this campaign. The experience acquired with M10 afterward during other campaigns and the willingness to use M10 radiosondes at several measurement stations of the GRUAN network, led to the development of the corrections that are presented in the section 3.

Seven Meteolabor Snow White (night models; 026 and 059 versions) soundings and 20 RS92 soundings were performed during the campaign (Table 1). In this study, we use these 20 soundings to apply the corrections to the M10 RH and perform comparisons with the RS92 RH profiles. For these soundings, the Vaisala DigiCORA III software, version 3.64, was used. No additional correction to the default corrections were applied to the RS92 data (Bock et al. 2013). According to the Vaisala data continuity website (https://www.vaisala.com/en/press-releases/2009-12/vaisala-launches-website-ensure-data-continuity-radiosounding-observations), the time lag, the daytime

TABLE 1. Radiosounding periods, characteristics, and software used for the SIRTA and OHP field experiments and for the routine measurements at the Trappes site.

Time	Period	Radiosondes	Software (radiosondes)	Raw sampling
		SIRTA		
Daytime, IOP	Oct and Nov 2016	7 dual soundings	IR2010 (M10); DigiCORA III (RS92)	1 s
Daytime, IOP	Jan 2018	10 dual soundings	Eoscan (M10); DigiCORA III (RS92)	1 s
Daytime, IOP	Jul and Aug 2018	12 dual soundings	Eoscan (M10); DigiCORA III (RS92)	1 s
		OHP		
Nighttime, IOP	Sept and Oct 2011	20 dual soundings	IR2010 (M10); DigiCORA III (RS92)	1 s
		Trappes		
2 times per day	Before 2007	Manual	DigiCORA III (RS92)	1 s
(1200 and 0000 UTC), routine	2007–15	Manual	IR2010 (M10)	
	After 2015	Automatic	IR2010 (M10)	

correction for solar heating, and the nighttime correction for radiative cooling started to be applied in December 2010 for standard RH data products recorded with DigiCORA 3.64 software. Because all measurements were performed at night during the OHP campaign, the only correction applied to RS92 humidity was the time-lag correction, the solar radiation algorithm having no impact on nighttime humidity (Jauhiainen et al. 2011). The accuracy of all of these corrections applied to the RS92 data used in this study in comparison with the GRUAN-corrected RS92 data is discussed in Yu et al. (2015).

c. *SIRTA field experiment*

The Instrumented Site for Atmospheric Remote Sensing Research (SIRTA) is a French national observatory dedicated to studying clouds, aerosols, dynamics and thermodynamics in the boundary layer and the free troposphere. The SIRTA observatory is a midlatitude site (48.7°N, 2.2°E) located in a semiurban area, on the Saclay plateau 25 km south of Paris (Haeffelin et al. 2005).

Three intensive observational periods (IOPs) dedicated to comparisons of vertical profiles of humidity were carried out between October 2016 and August 2018 with 29 M10–RS92 dual flights (see more details in Table 1). In this study, both IR2010 and Eoscan software were used to record the data measured and sent by the M10 radiosondes. IR2010 is the former software, which is still in used at several sites, whereas Eoscan is the new software from Meteomodem. For this study, we used the Eoscan and IR2010 programs solely to produce the raw data before any posttreatment. DigiCORA III software was used for the monitoring of the RS92 radiosondes and we allowed the standard corrections to be applied for the data considered in our study. The different corrections presented in section 3 are applied to the raw M10 data.

Standard ground checks were applied for M10 (ambient temperature and humidity chamber) and RS92 (temperature and 0% RH humidity chamber). For all of the figures, the altitude corresponds to the altitude above mean sea level.

3. Correction methods

Figure 3 shows a schematic overview of the correction methodology to convert the raw value of relative humidity to an optimized value taking into account the four corrections presented in the paper. Input parameters and related equations are indicated.

Meteomodem has developed one transfer function and performs an absolute calibration of the capacitance sensor that allows the conversion of the measured frequency into a relative humidity. This calibration can be verified a posteriori by measuring the relative humidity in conditions where the relative humidity is known. The sensor response time to a step change is highly dependent on temperature following a power law, yielding time constants that exceed 1 min when the temperature is below −55°C. Miloshevich et al. (2004) propose a response-time correction that we test and implement. It is observed that the capacitance relative humidity sensors are also affected by an additional slow-regime response time that has not been discussed in the literature. We present the concept and propose a correction method. Last, with regard to relative humidity bias due to spurious temperature of the sensor, often referred to as ''radiation dry bias,'' several authors (e.g., Vömel et al. 2007; Miloshevich et al. 2009; Dirksen et al. 2014) propose correction methods that depend on temperature and relative humidity or pressure. These methods are used and tested in the analysis of the data (section 3c).

a. *Absolute calibration correction*

The general process of calibration for the M10 radiosondes concerning the relative humidity sensor (RHS) follows two separate procedures. In the factory, each radiosonde

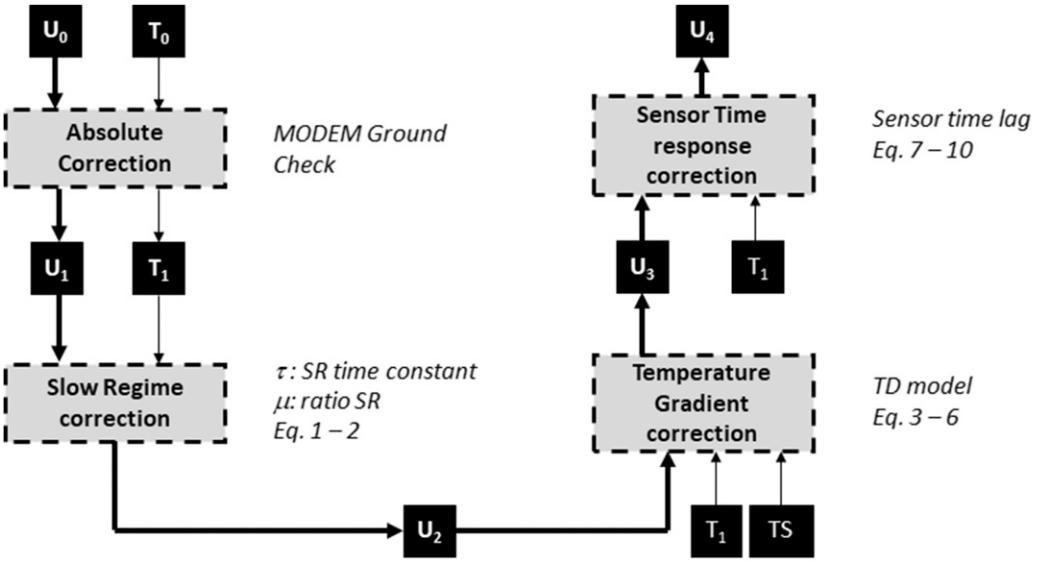

FIG. 3. Schematic overview of the correction method: TS is the temperature of the humidity sensor, U_0 is the raw humidity value, U_4 is the final humidity value after all of the corrections, T_0 is the raw temperature value, and T_1 is the air temperature after the absolute calibration if needed.

RHS is calibrated with a working humidity sensor at different temperature that is regularly calibrated against a reference standard. During the factory calibration, the temperature dependence of the relative humidity sensor is corrected with the temperature sensor. Hence, the calibration value is independent of the room temperature. The reference is traceable by an international standard through a sequence of measurement standards and calibrations [definition 2.42 Joint Committee for Guides in Metrology (JCGM) 200:2012]. Its place in the calibration hierarchy (definition 2.40 JCGM 200:2012) is two measurement standards from the international one. The general process of calibration for the M10 radiosondes concerning the RHS has been improved. This working standard is the same humidity sensor as that of the M10 radiosonde. It is verified at daily basis and calibrated if needed with respect to a reference standard. The reference standard is an HC2A-S Rotronic AG humidity sensor device (humidity and temperature HygroClip2 probe). It is calibrated every year by the Rotronic metrology services at 23°C for three different humidity levels (12%, 35%, and 80%), with respect to an HC2-S Rotronic humidity sensor device with a 2σ tolerance of $\pm 0.8\%$ RH between 10° and 30°C. The HC2-S device used by Rotronics is certified by the Swiss Calibration Service [SCS; accredited laboratory International Organization for Standardization/International Electrotechnical Commission (ISO/IEC) 17025]. The SCS is equipped to provide up to five predefined humidities in the 0.5%–85% RH range at 23°C with a accuracy better than 0.6% RH. It is also equipped with an air conditioned chamber allowing to test up to 20 different measurement ranges with a 2σ tolerance smaller that 2.1% RH (Accreditation Directory SCS0065). The M10 relative humidity sensor is calibrated for this 0.5%–85% RH range. According to Rotronics, the HC2S is traceable to an international standard through a documented and unbroken chain of calibrations. The HC2A-S used in the factory calibration process is compared four times per year with one other HC2A-S devices to verify the absence of measurement deviation. An additional verification procedure is carried out during the Meteomodem ground check before each launch. The ground check humidity sensor is calibrated with respect to a reference standard directly in laboratory conditions.

For this study, concerning the radiosondes launched during the OHP field experiment in 2011, a supplementary correction for calibration has been performed on each RH sounding record, which consists in making the assumption that the RH values converge to 0% at 30-km altitude, as expected. Each radiosonde has been verified individually to be sure that there is no contamination of the RH sensor by frozen water droplets. This correction had significant values for the case of the M10 radiosondes used in OHP campaign, which happened to be the prototype series used by Meteomodem for this type of radiosondes (M10 replaced the M2K2 radiosondes after that campaign) and for which issues during the early phases of the M10 radiosonde industrial production were encountered. This supplementary correction was not needed for the radiosondes used for the launches at SIRTA.

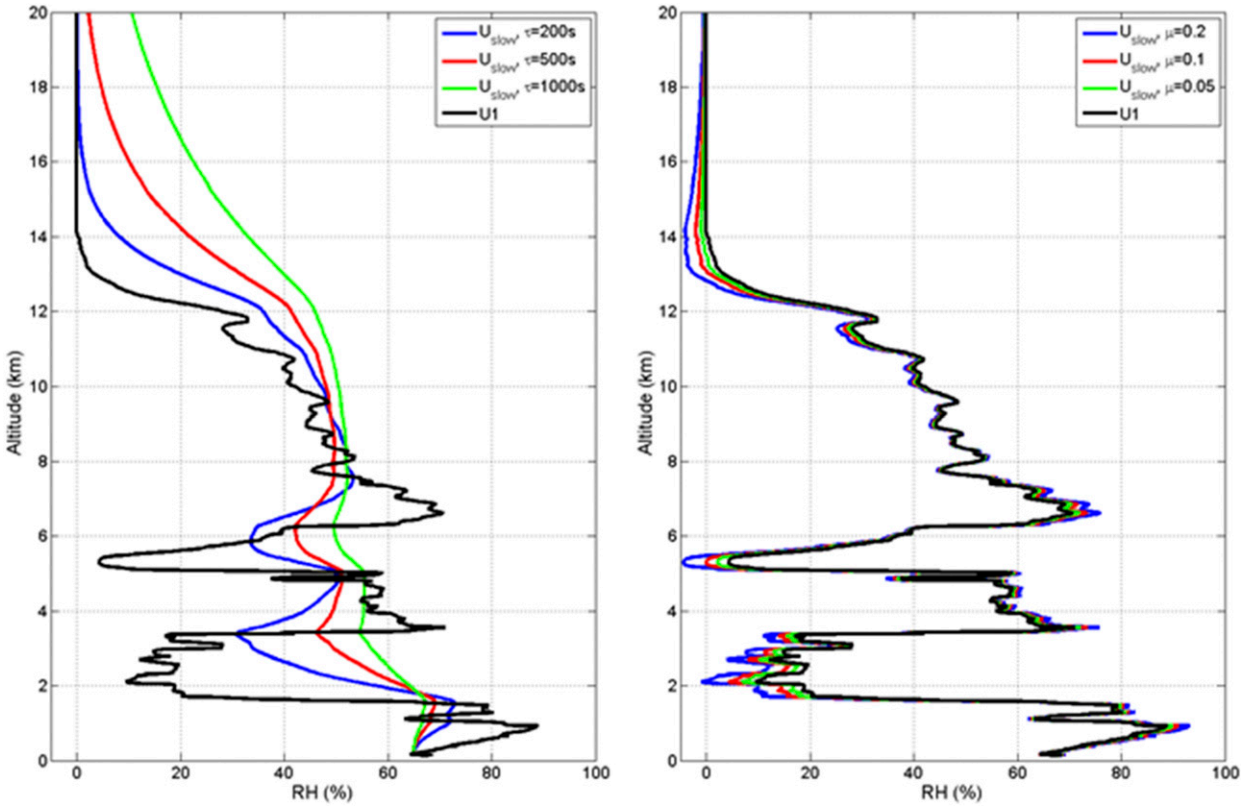

FIG. 4. Vertical profile of the raw relative humidity and relative humidity of the slow regime for (left) three time constants (τ = 200, 500, 1000 s), with a fixed ratio of the slow to fast response sensors μ = 0.1, and (right) three ratios of the slow to fast response sensors (μ = 0.2, 0.1, and 0.05) with a fixed time constant τ = 500 s at 0900 UT 24 Aug 2018 at the SIRTA observatory.

b. *Slow-regime correction*

A new method has been developed to take into account the effect inspired by the layered model of a capacitive humidity sensor proposed by Wildmann et al. (2014). Our method separates the response of the sensor to a step change in RH into a combination of two layers: a fast-regime layer and a slow-regime layer. The fast-regime layer corresponds to a fast change in humidity by more than 90% of the step change within a few seconds. The slow-regime layer represents a slow evolution of the measured humidity in the range of minutes for about 10% of the step change. To correct the measured humidity, a fraction of the difference between the measured humidity and the slow-regime layer is added to the measured humidity at each time step. We can define the corrected relative humidity U_2 as follows:

$$U_{2(i)} = U_{1(i)} + \mu[U_{1(i)} - U_{\text{slow}(i)}]\,, \qquad (1)$$

where U_{slow} is the relative humidity in the slow-regime layer, U_1 is the measured and uncorrected relative humidity, U_2 is the corrected relative humidity, μ is the fraction of the slow regime, and i is the index for a given position;

$$U_{\text{slow}(i)} = \frac{1}{\tau}[U_{1(i)} - U_{\text{slow}(i-1)}]\Delta t + U_{\text{slow}(i-1)}\,, \qquad (2)$$

where τ (in seconds) is the time constant of the slow-regime part of the sensor.

We have tested many combinations of τ and μ, and we show some examples in Fig. 4 [(120 and 0.2); (500 and 0.1); (1000 and 0.05)]. The left panel of Fig. 4 shows U_{slow} for different values of τ (120, 500, and 1000 s) with a constant μ = 0.1. The right panel of Fig. 4 shows U_{slow} for different values of μ (0.2, 0.1, and 0.05) with a constant τ = 500 s, for a particular example profile.

As expected, the higher the variation of relative humidity is, the more important the correction will be, especially for a small value of τ, that is, relatively fast response of the slow-regime layer, emphasized by an important μ. Slow-regime correction will be effective just after crossing a cloud under a dry air mass and, to a relatively smaller extent, after crossing the tropopause (see Fig. 4 at 1.8 and 12 km, respectively).

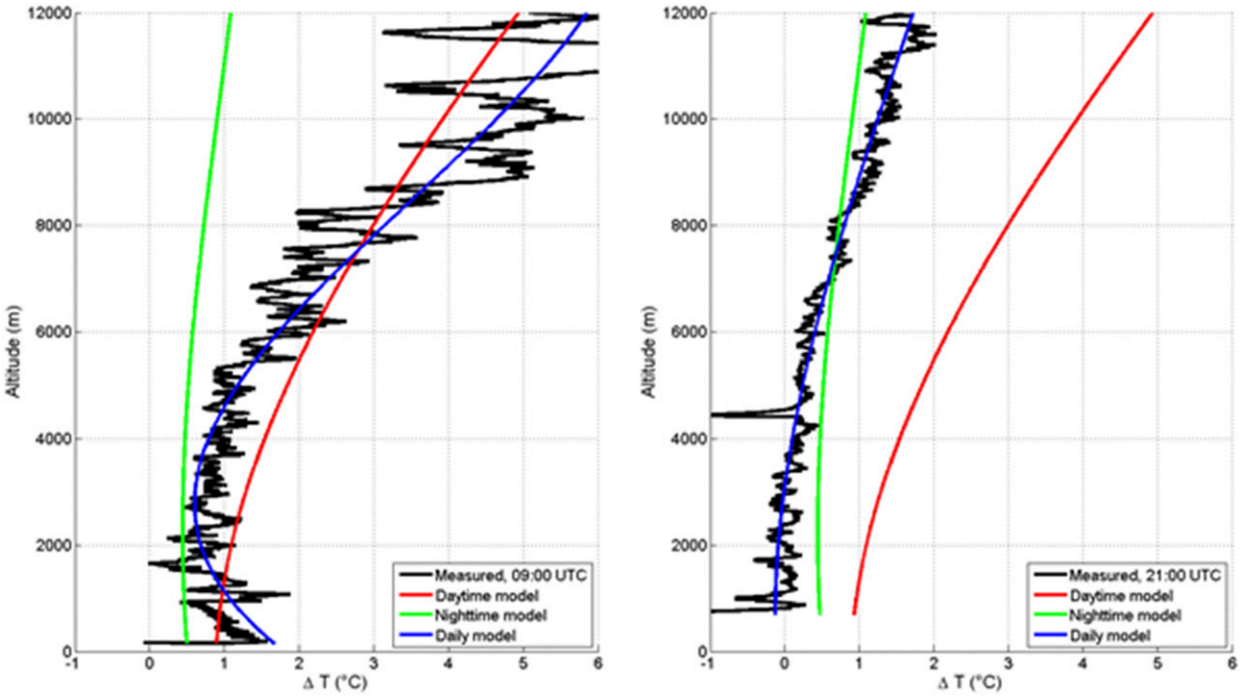

FIG. 5. Difference in temperature between the temperature close to the capacitive sensor and the air temperature sensor. The black line corresponds to the measured value, and the red, green, and blue lines correspond to the different models described in section 3c. Shown are radiosoundings launched at (left) the SIRTA observatory at 0900 UT 24 Aug 2018 and (right) the OHP at 2100 UT 21 Sep 2011.

c. *Temperature-gradient correction*

For a good measurement, the relative humidity should be measured when the capacitive sensor temperature and the air temperature are the same. However, multiple factors may hinder or contribute to break this equilibrium. During daytime measurements, as for the ones at the SIRTA observatory, the solar radiation can heat the sensor and create a dry bias in the humidity measurements, whereas during nighttime measurements, as at the OHP, the sensor is exposed to infrared radiation from Earth and from the surrounding water vapor and clouds. These radiative effects are modulated both in daytime and nighttime periods with the heat transferred by conduction to the sensor, from the radiosonde to the sensor boom and with the ventilation leading to a cooling effect.

Each of these factors has a variable influence on the sensor heat budget and, therefore, on its temperature. Indeed, radiative effects are very variable along the vertical due to the role of clouds on direct solar beam or on infrared cooling in relation with water vapor and hydrometeor spatial distribution. The ventilation of the sensor depends on the ascent speed, the distance between the radiosonde and the balloon and the induced pendulum motion, the presence of other radiosondes and their configuration under the balloon.

To evaluate the heating of the RHS, the approach undertaken for the M10 radiosondes was to take advantage of an available temperature measurement close to the RHS (hereinafter T_S) and to compare it with the measured temperature of the air T_1. Temperature T_S is measured on the sensor boom, 2 mm away from the RHS edge. Since the temperature sensor is not directly located on or inside the RHS, we can directly consider 1) the instantaneous value of the temperature difference between the air and the RHS (T_1 and T_s measurements) and 2) a fitted model based on T_1 and T_S. Figure 5 shows an example of this temperature difference profile ($T_S - T_1$, denoted as ΔT) at the SIRTA (Fig. 5, left panel) and OHP (Fig. 5, right panel) sites. The measured ΔT can be fitted with a polynomial fit as follows:

$$\Delta T = T_S - T_1 = \sum_{i=0}^{i=3} c_i z^i, \qquad (3)$$

where c_i *coefficients* are optimized by the least squares method, and z is the altitude above ground level in kilometers.

The c_i coefficients can be adjusted for each flight and for all the daytime or nighttime periods. The main advantage for this daily modeling is to have a better accuracy (see Fig. 5, blue lines), but the drawback is that we are obliged to await the end of the flight to process the ΔT. The main advantage of the climatological modeling is

TABLE 2. Parametrical coefficients for the daytime and nighttime models (2012–16 at Trappes) and for the two selected dates at SIRTA (24 Aug 2018) and OHP (21 Sep 2011).

Coef model	c_0	c_1	c_2	C_3
Daytime model	0.89	3.38×10^{-5}	3.53×10^{-8}	-8.35×10^{-13}
Nighttime model	0.51	5.82×10^{-5}	1.44×10^{-8}	-4.62×10^{-13}
SIRTA, 24 Aug 2018 (day)	1.81	-9.28×10^{-4}	2.00×10^{-7}	-7.84×10^{-12}
OHP, 21 Sep 2011 (night)	−0.12	-2.67×10^{-5}	2.30×10^{-8}	-6.63×10^{-13}

that we are ready to process ΔT at the beginning of the launch but the main drawback is that the uncertainty is bigger. In Fig. 5, the black line corresponds to the measured value; red, green and blue lines correspond to the different models (daily or climatological). Figure 5 (left panel) is a radiosounding launched at the SIRTA observatory at 0900 UT 24 August 2018; Fig. 5 (right panel) was launched at the OHP at 2100 UT 21 September 2011. Table 2 shows 1) the optimal parametrical coefficients for the daytime and nighttime climatological models obtained for the Trappes, France, radiosoundings between 2012 and 2016 (a total of 1800 radiosoundings at 1200 and 0000 UT), and 2) the coefficients for the two selected dates at SIRTA and OHP. For the climatological models, we have gridded all the profiles between the surface and 12 km of altitude with a vertical resolution of 50 m, and we optimized the parametrical coefficients by the least squares method. To account for the instantaneous effect of clouds, solar fluxes and convection effect that are shown on Fig. 5 (instantaneous variability reaching more than 10°C and a relative humidity correction exceeding more than 10%), we consider in this study the instantaneous value of the temperature difference between the air and the RHS rather than daily or annual parametrical model.

For the SIRTA radiosounding during daytime, the difference of temperature between the RH capacitive sensor and the air temperature sensor ranges from 0° to more than 6°C, at the surface and at 12 km, respectively. The solar radiation induces a difference that is strictly positive, with a humidity sensor warmer than the air, leading to a dry bias that needs to be corrected. To minimize the effect, the shield cover shades the humidity sensor. Because of its design, the humidity sensor is black, so it is expected that the influence of infrared radiation will be high, unlike air temperature sensor, which is covered by a metallic coating. The protection therefore shades the RH sensor to limit the effect of radiation. Its shape and design have been produced by Meteomodem.

For the OHP radiosounding during nighttime, ΔT ranges from −1° to +2°C, at the surface and around 12 km, respectively. The infrared radiative cooling associated with the dynamics around the M10 radiosonde induces alternatively a warming or a cooling of the humidity sensor. We note that the daily fit has a very good agreement with the measured ΔT whereas the climatological model can have discrepancies reaching 1° and 0.5°C for daytime and nighttime periods, respectively.

The estimation of the relative humidity sensor heating allows us to correct the observed humidity using the measured difference between the temperature of the capacitive sensor and the true temperature of the air. The relative humidity is defined as the ratio of the water vapor partial pressure e and the water vapor saturated pressure e_{sat} [Eq. (4), below]. The water vapor saturated pressure is a function of the temperature only;

$$U_{2(i)} = \frac{e_{2(i)}}{e_{\text{sat2}(i)}} \quad \text{and} \quad U_{3(i)} = \frac{e_{3(i)}}{e_{\text{sat3}(i)}}, \tag{4}$$

where the subscripts 2 and 3 correspond to two different locations on the sensor boom, and i is the index for a given position. The first corresponds to the location of the air temperature sensor (subscript 2), and the second corresponds to the location of the temperature sensor near the humidity sensor (subscript 3). Assuming that the water vapor partial pressure is uniform between these two locations (i.e., $e_2 = e_3$), Eq. (4) leads to

$$e_{2(i)} = e_{3(i)} \geq U_{3(i)} = U_{2(i)} \frac{e_{\text{sat2}(i)}}{e_{\text{sat3}(i)}}. \tag{5}$$

The Hyland and Wexler law (Hyland and Wexler 1983) leads to

$$K = \frac{e_{\text{sat2}(i)}}{e_{\text{sat3}(i)}} = \left[\frac{T_{2(i)}}{T_{S(i)}}\right]^E \exp\left\{A\left[\frac{1}{T_{2(i)}} - \frac{1}{T_{S(i)}}\right] + B\left[T_{2(i)} - T_{S(i)}\right] + C\left[T_{2(i)}^2 - T_{S(i)}^2\right] + D\left[T_{2(i)}^3 - T_{S(i)}^3\right]\right\}, \tag{6}$$

where $T_{2(i)}$ is the air temperature sensor in kelvins, $T_{S(i)}$ is the temperature sensor near the humidity sensor in kelvins, A is equal to -0.580×10^4, B is equal to -0.0486, C is equal to $+0.418 \times 10^{-4}$, D is equal to -0.145×10^{-7}, E is equal to $+6.546$, and i is the index for a given position.

We tested 10 different formulations of water vapor partial pressure over liquid water and decided to select the abovementioned Hyland and Wexler law (Hyland and Wexler 1983). For a 2°C heating, which is a typical value of ΔT at 6 km for daytime periods, K is around 1.25. Likewise for a 4°C heating, which is a typical value of ΔT at 10 km for daytime periods, K is around 1.5. The impact on the vertical profile of humidity can also be very significant, particularly for high altitude.

d. Sensor-response-time correction

The time constant of capacitance sensors to a step input change is typically of less than 1 s at 20°C. The radiosonde ascent speed is typically 5 m s^{-1}; hence, a 1-s time response would be sufficient to monitor the abrupt changes in relative humidity observed in the atmosphere at the top of the boundary layer or at cloud boundaries. However, the time constant increases significantly at colder temperatures, exceeding 30 s at temperatures below −40°C according to Meteomodem. Because the response time increases with decreasing temperature, sharp relative humidity changes in the upper troposphere and lower stratosphere are likely to be reported by the radiosonde at a later time than they truly occur. This effect must be corrected.

Miloshevich et al. (2004) documented an approach to correct the response time for the Vaisala RS80 humidity sensor in which the response is an exponential function of time [see Eq. (3) in Miloshevich et al. 2004]. Dirksen et al. (2014) more recently developed a correction for the RS92 sensor in which the sensor response time of the humidity sensor is an exponential function of the temperature. Although the response-time effect is common to all capacitive sensors, the relative humidity sensor time-constant temperature dependences of two different sensors are likely not to be the same.

Considering the relative humidity sensor as a first-order low-pass filter, the measured relative humidity can be expressed as

$$U_{3(i)} = U_{3(i-1)} + k\left[U_{4(i)} - U_{3(i-1)}\right], \tag{7}$$

where U_3 is the measured relative humidity, U_4 is the final relative humidity after all of the corrections, k is the gain factor, and i is the index for a given position.

This equation can be mathematically rewritten, expressing U_4 as a function of the measured relative humidity slope:

$$U_{4(i)} = \tau_{[T(i)]}\frac{U_{1(i+N)} - U_{1(i-N)}}{2N_{[T(i)]}} + U_{3(i)}, \tag{8}$$

where $\tau_{(T)}$ is the temperature-dependent time constant of the sensor [see Eq. (10), below], N is the number of measurements used to derived the slope, and i is the index for a given altitude. This number N depends on the temperature and is defined as

$$N_{[T(i)]} = \alpha_1\left[T_{1(i)}/\beta_1\right]^{\gamma_1}, \tag{9}$$

where $\alpha_1 = 20$, $\gamma_1 = 4$, and $\beta_1 = 60$; N ranges from $N_{(T>0°C)} = 5$ s to $N_{(T<-60°C)} = 120$ s to prevent extreme values at low altitude and in the upper troposphere.

Time constant values are provided by Meteomodem (from laboratory tests) for temperatures ranging +20° to −40°C (see black circles in Fig. 6, left panel). They are not provided at lower temperatures, for which an empirical approach was used to derive the $\tau_{(T)}$ relation. For this, some radiosoundings performed by MeteoFrance at Trappes were used. The method retrieves τ around the tropopause, where temperatures can be as low as −70°C at midlatitudes, by comparing the measurements during radiosonde ascent and descent at this altitude. The soundings were selected following three criteria:

1) nighttime soundings only, to avoid an additional effect from solar radiation,
2) a small stratospheric drift, to maximize the chances to probe the same temperature and humidity when passing upward and downward at the tropopause, and
3) a neat humidity drop at the tropopause level; for this, cases of deep convection were discarded to have stable conditions between upward and downward situations.

During both the ascent and descent of the radiosonde, the measured RH at the tropopause level was corrected following Eq. (10). The left panel of Fig. 6 shows values provided by Meteomodem and the values derived from the experimental method. The value of τ [Eqs. (8) and (10)] is changed by iteration to minimize "d," the Euclidean distance between the ascent and descent corrected curves around the tropopause.

To take into account these points and the ranges, a curve was derived using the following equation:

$$\tau_{[T(i)]} = \alpha\left[T_{1(i)}/\beta\right]^{\gamma}, \tag{10}$$

where the values for the coefficients are $\alpha = 90$, $\gamma = 4$, and $\beta = 60$.

This method turns out to be a useful evaluation technique as an alternative to a retrieval of the RHS

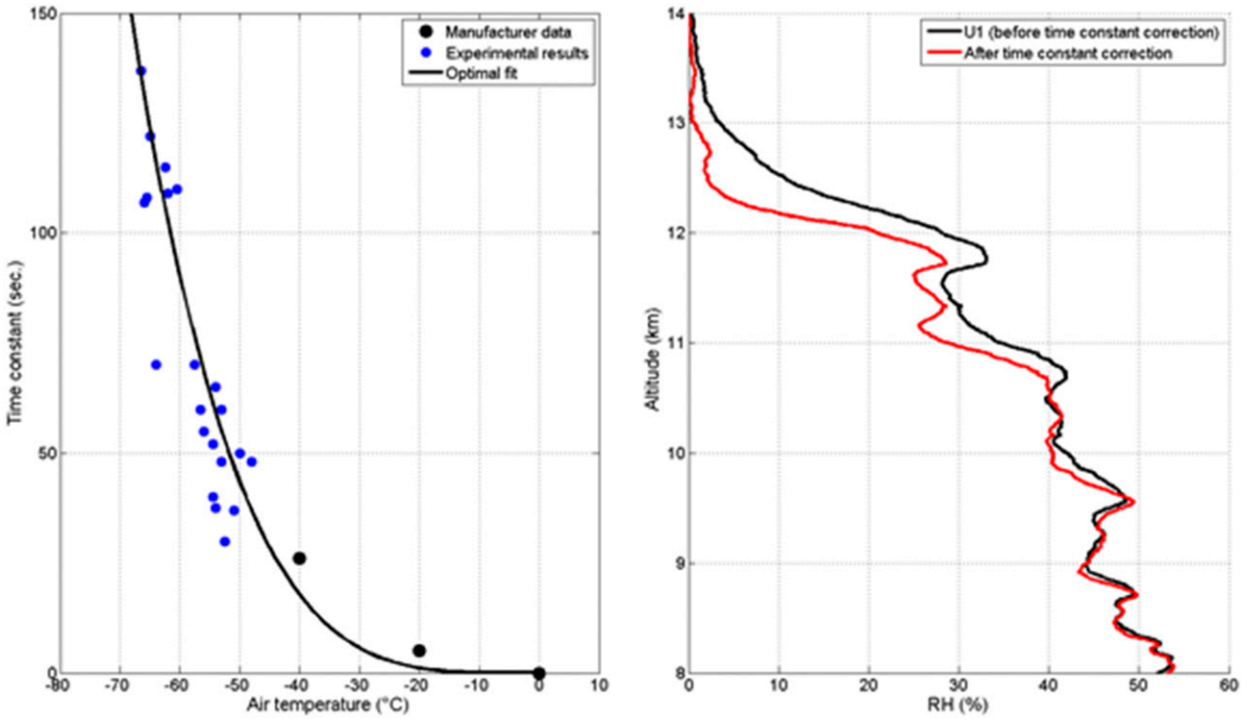

FIG. 6. (left) The temperature dependence of the M10 humidity sensor time constant: blue symbols are experimental values as explained in section 3d, black symbols are Meteomodem data, and the black line is the optimal polynomial fit. (right) The impact of this time constant on the vertical profile of humidity on 24 Aug 2018 at the SIRTA observatory: the black and red lines correspond to the data before and after the time constant correction, respectively.

response time in the laboratory. It is important to stress that the temperature dependence expression (Fig. 6, left panel) derived here is an evaluation of the RHS time-lag behavior with measured air temperature. Indeed, Meteomodem points at −40° and −20°C are not perfectly superimposed to the curve. Neither are some of the experimental points. A compromise was then adopted to optimize the three parametrical coefficients to the complete dataset.

Figure 6 (right panel) shows an example of the application of the time-lag correction on the RH measurements from 8 to 14 km of altitude for a M10 radiosounding. The black and red curves are, respectively, the RH before and after the time-lag correction. The correction is seen to enhance the slopes and the amplitudes of the peaks.

4. Sensitivity tests and statistics

a. *Sensitivity tests*

We have presented in section 3 the method to optimize the M10 radiosonde profiling with three main corrections. The first correction, hereinafter "slow-regime correction," depends on two parameters τ and μ. The second correction, hereinafter "temperature-gradient correction," is related to the period during which the temperature offset is fitted (daily, climatological) or measured (instantaneous). The third correction, hereinafter "sensor-response-time correction," is directly fitted with a previous dataset.

We estimate the impact of each successive corrections of M10 relative humidity (U_1, U_2, U_3, and U_4) in comparison with RS92 relative humidity. In Tables 3 and 4, we report a global correction effect difference constructed as the absolute mean over all the flights and altitudes on an interpolated 50 m grid. The RS92 dataset has been used to develop the three main corrections on M10 radiosonde, and this dataset validates the new M10 dataset.

Table 3 corresponds to the data collected at the SIRTA observatory with 25 radiosondes during the daytime periods. The initial difference in relative humidity between M10 and RS92 is around 5.4% RH with a standard deviation of 1.8% RH. The impact of τ and μ appears directly on U_2, but the final impact on U_4 is very significant (U_4 ranges from 3.9% to 5.1% RH on average). The standard deviation is also divided by 2 between U_1 and U_4. The best configuration corresponds to $\tau = 500$ s and $\mu = 0.1$ for a measured temperature gradient with a final mean difference of 3.9% ± 0.8%

TABLE 3. Mean value and standard deviation of the absolute difference between relative humidity provided by M10 radiosondes (U_1, U_2, U_3, and U_4) and provided by RS92 for different configurations of corrections. The results correspond to the SIRTA field experiment (25 daytime profiles). The best configuration is indicated by boldface type.

Parameters	$\lvert U_1 - U_{RS92}\rvert$	$\lvert U_2 - U_{RS92}\rvert$	$\lvert U_3 - U_{RS92}\rvert$	$\lvert U_4 - U_{RS92}\rvert$
τ = 500 s, μ = 0.1, and measured temperature gradient	**5.4 ± 1.8**	**4.8 ± 1.9**	**4.5 ± 0.9**	**3.9 ± 0.8**
τ = 200 s, μ = 0.1, and daily temperature model	5.4 ± 1.8	5.0 ± 1.9	5. ± 1.0	5.1 ± 0.9
τ = 1000 s, μ = 0.1, and daily temperature model	5.4 ± 1.8	4.8 ± 2.0	4.6 ± 0.9	4.1 ± 0.8
τ = 500 s, μ = 0.2, and daily temperature model	5.4 ± 1.8	4.8 ± 1.9	5.0 ± 1.0	4.5 ± 0.9
τ = 500 s, μ = 0.05, and daily temperature model	5.4 ± 1.8	5.1 ± 1.9	5.6 ± 1.1	5.0 ± 0.9
τ = 500 s, μ = 0.1, and daytime temperature model	5.4 ± 1.8	4.8 ± 2.0	5.9 ± 1.2	5.4 ± 1.1
τ = 500 s, μ = 0.1, and nighttime temperature model	5.4 ± 1.8	4.8 ± 2.0	4.2 ± 1.5	4.0 ± 1.8

RH. The daytime climatological model dedicated to fit with the temperature correction leads to a decrease in the standard deviation to 1.1% RH, and the average bias decreases from 5.4% to 3.9% RH.

Table 4 is the same as Table 3 but for the OHP field experiment with 20 nighttime radiosoundings. The initial bias is equal to 3.2% RH with a standard deviation of 1.1% RH. The same configuration of parameters (τ = 500 s and μ = 0.1) is used to reach the minimum bias (1.7% RH) and standard deviation (0.6% RH), which both decrease by a factor 2.

Figure 7 shows the vertical profile of slow-regime correction (left panels), temperature correction (center panels), and time-lag correction (right panels) for the 25 radiosoundings launched at the SIRTA observatory (Fig. 7, top panels) and for the 20 radiosoundings launched at the OHP (Fig. 7, bottom panels). The average value is plotted as a solid line, and the standard deviation is shown with dashed lines. The slow-regime correction depends on the difference between the humidity in the slow reservoir and the measured humidity. Its impact is more perceptible when RH changes are fast and important. The slow-regime correction subtracts a maximum of around 2.5% of RH at 5 km for the SIRTA profiles, and adds 2.5% of RH at 1 km and subtracts 1% of RH at 3 km for the OHP profiles. At higher altitudes, the slow-regime correction is smaller than 1% of RH. The curves in the center panels of Fig. 7 show the mean impact of the temperature-gradient correction. For the SIRTA field experiment (i.e., for daytime flights), between the ground and 5 km, this correction is around +3%–4%, meaning that on average the relative humidity sensor was warmer than the air at these altitudes with a relatively constant offset. Above 5 km, the mean impact of the correction increases and peaks at 10 km with +12% RH as a result of the solar heat flux associated with a high value of relative humidity (see section 4b), then decreases to 0% RH at 13 km, where the atmospheric relative humidity tends to 0% RH. For the OHP field experiment (i.e., for nighttime flights), this correction ranges from 0% RH at 5 km to 3% RH at 12 km or to 1% RH at 15 km in relation to the absence of solar heating.

The curves in the right panels of Fig. 7 show the impact of the time-lag correction. Up to 7 km, the correction is zero because the temperature is higher than −40°C, so that the sensor is still responding fast (see Fig. 6). Above this altitude, the correction can lead to an increase or decrease in RH, depending on each single profile slope (Fig. 6). The correction maximizes around 10–12 km for SIRTA and 11–13 km for OHP, corresponding to the fast relative humidity drop near the tropopause, with a maximum mean effect of −3% RH for SIRTA and −4% RH for OHP.

b. *Final profiles*

In Fig. 8, the black curve shows the mean impact of the slow-regime correction, the green curve shows the mean impact of the temperature-gradient correction, and the red curve shows the impact of the time-lag correction.

TABLE 4. As in Table 3, but for the OHP field experiment (20 nighttime profiles).

Parameters	$\lvert U_1\text{-}U_{RS92}\rvert$	$\lvert U_2\text{-}U_{RS92}\rvert$	$\lvert U_3\text{-}U_{RS92}\rvert$	$\lvert U_4\text{-}U_{RS92}\rvert$
τ = 500 s, μ = 0.1, and measured temperature gradient	**3.2 ± 1.1**	**2.7 ± 1.1**	**2.6 ± 1.3**	**1.7 ± 0.6**
τ = 200 s, μ = 0.1, and daily temperature model	3.2 ± 1.1	2.8 ± 1.1	2.6 ± 1.2	1.8 ± 0.6
τ = 1000 s, μ = 0.1, and daily temperature model	3.2 ± 1.1	2.7 ± 1.1	2.6 ± 1.3	1.7 ± 0.6
τ = 500 s, μ = 0.2, and daily temperature model	3.2 ± 1.1	2.9 ± 1.0	2.8 ± 1.2	2.1 ± 0.6
τ = 500 s, μ = 0.05, and daily temperature model	3.2 ± 1.1	2.9 ± 1.1	2.7 ± 1.2	1.8 ± 0.7
τ = 500 s, μ = 0.1, and daytime temperature model	3.2 ± 1.1	2.7 ± 1.1	7.1 ± 2.4	6.3 ± 1.9
τ = 500 s, μ = 0.1, and nighttime temperature model	3.2 ± 1.1	2.7 ± 1.1	2.2 ± 1.1	1.6 ± 0.8

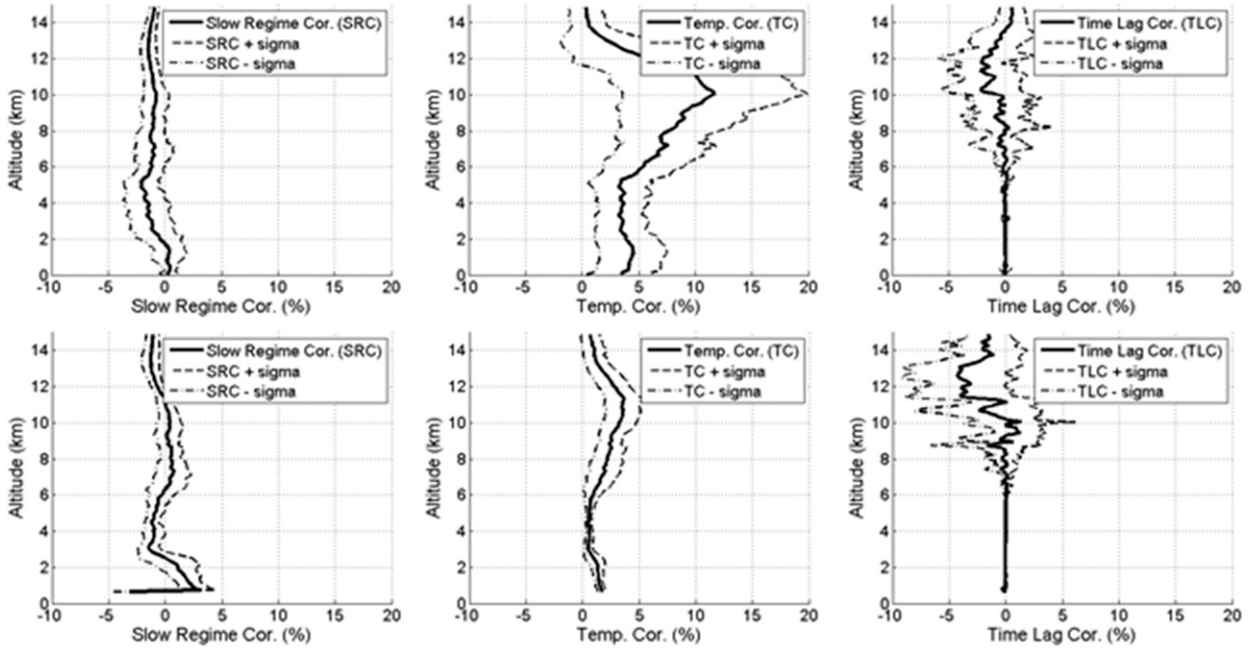

FIG. 7. Vertical profile of (left) the slow-regime correction, (center) the temperature correction, and (right) the time-lag correction for (top) the 25 radiosoundings launched at the SIRTA observatory for the daytime period and (bottom) the 20 radiosoundings launched at the OHP Observatory for the nighttime period. The average value is plotted as a thick line, and the standard deviation is shown with dashed lines.

The blue line corresponds to the vertical profile of relative humidity difference between the M10 sensor before all of the corrections and the RS92 sensor. The cyan line corresponds to the vertical profile of relative humidity difference between the M10 sensor after all of the corrections and the RS92 sensor. For all of these corrections, the mean impact is processed after an interpolation to a 50-m vertical grid between the surface and the maximum altitude for which both radiosondes (M10 and RS92) have reported measurements.

For the SIRTA field experiment, the initial (before the corrections) maximal difference is around −8% near the ground level, +3% RH at 5 km, and −6% RH at 10 km. After all of the corrections, this difference is around −4% near the ground level and reaches +5% at 7 km. For the OHP field experiment, the initial maximal difference is −3% RH at 1.5 km and reaches −6.5% RH at 11.5 km. After all of the corrections, the difference ranges between −2% and +2% RH.

Figure 9 shows the mean relative humidity profiles and standard deviations for M10 (blue) and RS92 (red) interpolated on a 50-m vertical grid, for SIRTA (Fig. 9, left panel) and OHP (Fig. 9, right panel) field experiments. The mean difference is smaller (with respect to each single flight) with a high stability of the difference (a low standard deviation relative to the first series of M10 data; Bock et al. 2013). The correction is much more efficient for nighttime profiles (OHP campaign) in relation with the temperature gradient that is very low for nighttime periods. For the daytime profile obtained during the SIRTA field experiment, the most important difference between M10 and RS92 ($RH_{M10} > RH_{RS92}$) appears between 5 and 10 km, where a lot of cirrus clouds occur during the different field experiments. In some events, the temperature-gradient correction can have a too strong impact on the relative humidity profiles compared to the RS92 radiosonde.

5. Conclusions

A set of corrections for M10 RH has been developed and tested for two field experiments, one with daytime launches at the SIRTA observatory and one with nighttime launches at the OHP. The corrections are based on observed physical phenomena and postprocessing verification. The corrections applied on the dataset are the following:

1) a correction for calibration, applied to the raw data of the OHP campaign (necessary because of a calibration bias in the early series of M10 radiosondes),
2) a slow-regime correction, based on the observed behavior of the sensor when responding to a step change in RH,

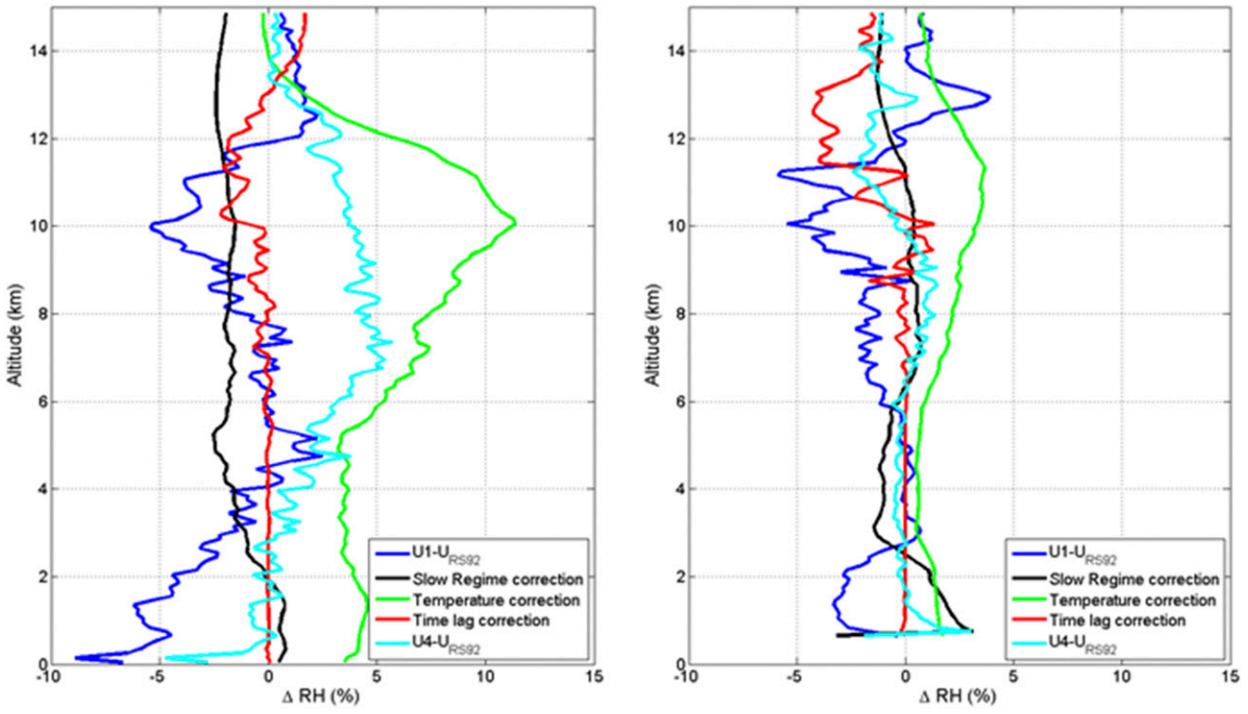

FIG. 8. Average contribution of each correction (slow regime, black; temperature, green; time lag, red) to the vertical profile of relative humidity (raw data in blue, and final result in cyan) for (left) the 25 radiosoundings launched at SIRTA for the daytime period and (right) the 20 radiosoundings launched at OHP for the nighttime period.

3) a temperature-gradient correction, which is based on the estimation of the difference between the RH sensor temperature and the actual air temperature, and
4) a time-lag correction, which improves the RH sensor response at very low temperatures.

The corrections have been applied to the whole M10 dataset and the impact of each correction on the M10 relative humidity profile has been quantified.

As mentioned by Bock et al. (2013), the M10 used during the OHP campaign was a very recent product at the time. These radiosondes were actually the very first series that had been produced. The calibration issues encountered then, because of the early production stage, have a priori no link with the physical nature of the M10 relative humidity sensor.

The three remaining corrections are based on physical phenomena. The time-lag correction and the slow-regime correction have comparable amplitude for day and night periods, but the time-lag impact is much more significant at high altitude (above 10 km) whereas the slow regime affects the relative humidity in the lower to middle atmosphere (below 7 km).

The time lag affects all capacitive relative humidity sensors and is due to the temperature dependence of the sensor response time at temperatures lower than approximately −40°C. Here, an original method using ascent and descent profiles has been used to derive an estimation of the dependency of the sensor response time to temperature.

The temperature-gradient correction uses a temperature measurement that is done near (2 mm away) the RHS. The magnitude of the correction factor depends on the measured temperature difference between the air and the sensor. It allows a correction of the measured RH, which can be positive or negative depending on the sign of the difference.

The observed slow reaction of the RH sensor when submitted to a relative humidity step change has motivated the development of a slow-response correction. This correction is based on the assumption that the propagation of water vapor molecules inside the relative humidity sensor can be explained with the diffusion theory equations.

Meteomodem developed a transfer function and performs an absolute calibration of the capacitance sensor that allows the conversion of the measured frequency into a relative humidity. This calibration can be verified a posteriori by measuring the relative humidity in conditions where the relative humidity is known. The sensor response time to a step change is highly dependent on temperature following a power law, yielding time constants that exceed 1 min when

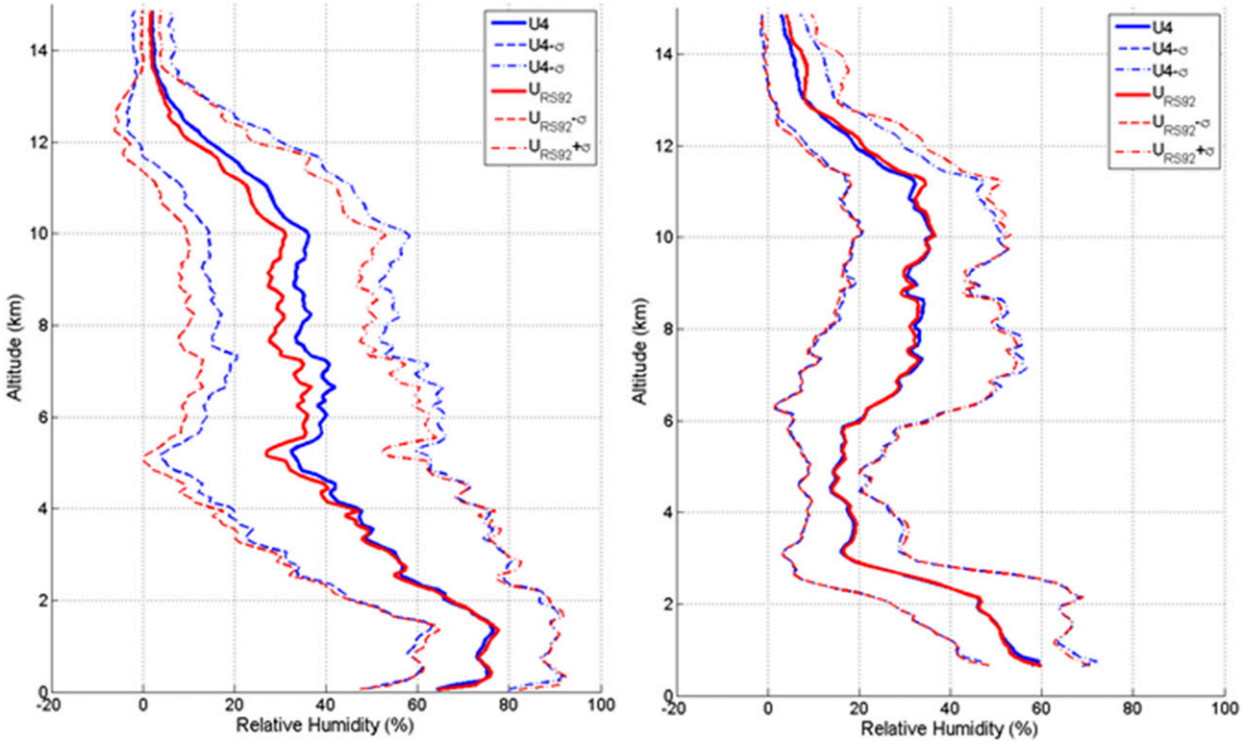

FIG. 9. Mean relative humidity profiles and standard deviations for M10 (blue) and RS92 (red) interpolated on a 50-m vertical grid, for the (left) SIRTA and (right) OHP field experiments.

the temperature is below −55°C. Miloshevich et al. (2004) propose a response-time correction that we test and implement. It is observed that the capacitance relative humidity sensors are also affected by another effect that can be explain by an additional slow-regime response time that has not been discussed in the literature. We present the concept and propose a correction method. With regard to relative humidity bias due to spurious temperature of the sensor, often referred to "radiation dry bias," several authors (e.g., Vömel et al. 2007; Miloshevich et al. 2009; Dirksen et al. 2014) propose correction methods that depend on temperature and relative humidity or pressure. We test and implement such methods.

The average RH profiles measured by M10 and RS92 have been compared after each correction has been applied to the M10 observations. The remaining difference between the two sensors is lower than 1.7% RH and 3.9% RH for the OHP and SIRTA field experiments, respectively.

In a future work, we will use these three main corrections to evaluate the Meteomodem M10 final products with 1) the GRUAN-corrected RS92 dataset, 2) a Snow White radiosonde, and 3) a cryogenic frost-point hygrometer (CFH) radiosonde for more than 10 dual flights conducted at Réunion Island between 2017 and 2019.

Acknowledgments. The authors thank the technical and computer staff of the SIRTA and OHP for taking the observations and making the dataset easily accessible. The authors acknowledge MeteoFrance for providing the Trappes radiosonde data, the ACTRIS-FR and DEMEVAP projects for funding a part of the field experiments, and IPSL federative infrastructure for article funding.

REFERENCES

Balagurov, A., A. Kats, and N. Krestyannikova, 1998: Implementation and results of the WMO radiosonde humidity sensors intercomparison (phase I laboratory test). *Tech. Conf. on Meteorological and Environmental Instruments and Methods of Observation*, Casablanca, Morocco, WMO, 181–184.

Bock, O., and Coauthors, 2013: Accuracy assessment of water vapour measurements from in situ and remote sensing techniques during the DEMEVAP 2011 campaign at OHP. *Atmos. Meas. Tech.*, **6**, 2777–2802, https://doi.org/10.5194/amt-6-2777-2013.

Bojinski, S., M. Verstraete, T. C. Peterson, C. Richter, A. Simmons, and M. Zemp, 2014: The concept of essential climate variables in support of climate research, applications, and policy. *Bull. Amer. Meteor. Soc.*, **95**, 1431–1443, https://doi.org/10.1175/BAMS-D-13-00047.1.

Dirksen, R. J., M. Sommer, F. J. Immler, D. F. Hurst, R. Kivi, and H. Vömel, 2014: Reference quality upper-air measurements: GRUAN data processing for the Vaisala RS92 radiosonde.

Atmos. Meas. Tech., **7**, 4463–4490, https://doi.org/10.5194/amt-7-4463-2014.

Elliott, W. P., R. J. Ross, and W. H. Blackmore, 2002: Recent changes in NWS upper-air observations with emphasis on changes from VIZ to Vaisala radiosondes. *Bull. Amer. Meteor. Soc.*, **83**, 1003–1017, https://doi.org/10.1175/1520-0477(2002)083<1003:RCINUA>2.3.CO;2.

Haeffelin, M., and Coauthors, 2005: SIRTA, a ground-based atmospheric observatory for cloud and aerosol research. *Ann. Geophys.*, **23**, 253–275, https://doi.org/10.5194/angeo-23-253-2005.

Hyland, R. W., and A. Wexler, 1983: Formulations for the thermodynamic properties of the saturated phases of H_2O from 173.15 K to 473.15 K. *ASHRAE Trans.*, **89** (2A), 500–519, https://www.techstreet.com/ashrae/standards/dc-2793-rp-216-formulations-for-the-thermodynamic-properties-of-the-saturated-phases-of-h2o-from-173-5-k-to-473-5-k?product_id=1836746.

Jauhiainen, H., M. Turunen, and J. Währn, 2011: Improved measurement accuracy of Vaisala radiosonde RS92. *Vaisala News*, No. 185, Vaisala, Helsinki, Finland, 4–7, https://www.vaisala.com/en/file/13201/download?token=DKVptaO9.

Kizu, N., T. Sugidachi, E. Kobayashi, S. Hoshino, K. Shimizu, R. Maeda, and M. Fujiwara, 2018: Technical characteristics and GRUAN data processing for the Meisei RS-11G and iMS-100 radiosondes. Hokkaido University Tech. Doc. GRUAN-TD-5, Rev. 1.0 (2018-02-21), 152 pp.

Matsuguchi, M., T. Kuroiwa, T. Miyagishi, S. Suzuki, T. Ogura, and Y. Sakai, 1998: Stability and reliability of capacitive-type relative humidity sensors using crosslinked polyimide films. *Sens. Actuators*, **52B**, 53–57, https://doi.org/10.1016/S0925-4005(98)00255-X.

Miloshevich, L. M., H. Vömel, A. Paukkunen, A. J. Heymsfield, and S. J. Oltmans, 2001: Characterization and correction of relative humidity measurements from Vaisala RS80-A radiosondes at cold temperatures. *J. Atmos. Oceanic Technol.*, **18**, 135–156, https://doi.org/10.1175/1520-0426(2001)018<0135:CACORH>2.0.CO;2.

——, A. Paukkunen, H. Vomel, and S. J. Oltmans, 2004: Development and validation of a time-lag correction for Vaisala radiosonde humidity measurements. *J. Atmos. Oceanic Technol.*, **21**, 1305–1327, https://doi.org/10.1175/1520-0426(2004)021<1305:DAVOAT>2.0.CO;2.

——, H. Vömel, D. N. Whiteman, and T. Leblanc, 2009: Accuracy assessment and correction of Vaisala RS92 radiosonde humidity measurements. *J. Geophys. Res.*, **114**, D11303, https://doi.org/10.1029/2008JD011565.

Seidel, D. J., and Coauthors, 2009: Reference upper-air observations for climate: Rationale, progress, and plans. *Bull. Amer. Meteor. Soc.*, **90**, 361–369, https://doi.org/10.1175/2008BAMS2540.1.

Vömel, H., and Coauthors, 2007: Radiation dry bias of the Vaisala RS92 humidity sensor. *J. Atmos. Oceanic Technol.*, **24**, 953–963, https://doi.org/10.1175/JTECH2019.1.

Wildmann, N., F. Kaufmann, and J. Bange, 2014: An inverse-modelling approach for frequency response correction of capacitive humidity sensors in ABL research with small remotely piloted aircraft (RPA). *Atmos. Meas. Tech.*, **7**, 3059–3069, https://doi.org/10.5194/amt-7-3059-2014.

Yu, H., P. E. Ciesielski, J. Wang, H.-C. Kuo, H. Vomel, and R. Dirksen, 2015: Evaluation of humidity correction methods for Vaisala RS92 tropical sounding data. *J. Atmos. Ocean. Tech.*, **32**, 397–411, https://doi.org/10.1175/JTECH-D-14-00166.1.

Zou, X., L. Lin, and F. Weng, 2013: Absolute calibration of ATMS upper level temperature sounding channels using GPS RO observations. *IEEE Trans. Geosci. Remote Sens.*, **52**, 1397–1406, https://doi.org/10.1109/TGRS.2013.2250981.